Turkish Journal of Civil Engineering, 2023 1-25, Paper 738, ***Research Article***

Investigation of Pounding between Two Adjacent Building Models with Experimental Methods

Çağla ŞEKERCI[1]
Erdem DAMCI[2]

ABSTRACT

This study investigates the pounding phenomenon by shaking table experiments on two scaled building models. Representing the situation where the seismic gap is insufficient, two building models are adjacently positioned on the shaking table, and pounding was investigated for harmonic and strong ground motion excitations. Displacement and acceleration responses were obtained to observe the pounding effect experimentally from video and accelerometer recordings, respectively. The Kelvin-Voigt Model consisting of spring and damper was used for numerical pounding analysis. The most critical parameters of the Kelvin–Voigt model, which are the spring stiffness (k_s) and the damping calculated according to the coefficient of restitution (r) were investigated and compared with harmonic experimental results. The obtained parameters, compatible with the harmonic experiments, were used to examine structural behavior under earthquake effect for the case where the building models are positioned for an insufficient seismic gap. For comparison, numerous numerical simulations were realized using different spring stiffnesses and coefficients of restitution. The study shows that when the coefficient of restitution is taken as 0.2 or 0.4, and the ratio of spring stiffness to shear stiffness (k_s/k) is 1 or 5, reasonable results in numerical earthquake simulations can be obtained.

Keywords: Pounding, Kelvin-Voigt model, image-processing, shaking table experiments, seismic gap.

1. INTRODUCTION

In countries located in earthquake zones, especially in big cities, as in the past, most buildings constructed today are built adjacently due to subdivisions and city planning works. The width of the seismic gap, which must be provided between existing or new adjacent buildings, is of

Note:
- This paper was received on December 15, 2021 and accepted for publication by the Editorial Board on April 14, 2023.
- Discussions on this paper will be accepted by September 30, 2023.
- https://doi.org/10.18400/tjce.1287522

1 Istanbul University-Cerrahpasa, Department of Civil Engineering, Istanbul, Turkey
Dogus University, Department of Civil Engineering, Istanbul, Turkey
cagla.sekerci@ogr.iuc.edu.tr - csekerci@dogus.edu.tr - https://orcid.org/0000-0001-7070-1804

2 Istanbul University-Cerrahpasa, Department of Civil Engineering, Istanbul, Turkey
edamci@iuc.edu.tr - https://orcid.org/0000-0003-2295-1686

great importance. While designing and analyzing the buildings, the effect on adjacent buildings is generally not considered in cases where the widths foreseen for the seismic gap are insufficient or not available. Modern seismic codes have regulations for seismic gap sizes to overcome this problem. Miari et al. [1], in their review article, summarized the criteria regarding the seismic gap in current seismic codes and investigations on this subject. In addition to these codes, there are restrictions for seismic gaps in the Turkish Building Earthquake Code 2018 (TBEC 2018) [2]. In this code, it is foreseen that the minimum seismic gap size for buildings up to 6 m in height should be at least 30 mm and at least adding 10 mm for each 3 m height. In addition, an empirical relation is presented over the calculated displacements of adjacent structures, and a limitation is introduced. Pounding, which could occur due to an insufficient seismic gap, is an issue that needs to be examined in terms of structural dynamics and earthquake engineering. For this purpose, there are several numerical but limited experimental studies in the literature on subjects such as the pounding force between two adjacent structures, the number of pounding, the moment of collision, and the determination and investigation of the size of the seismic gap [3-8, 10].

Studies in the literature for simplified structural models, pounding models only include numerical models created by using spring or spring-damper elements together. The main ones of these numeric models are elastic impact element, Kelvin-Voigt (Linear Viscoelastic), Modified Kelvin-Voigt, Non-Linear Viscoelastic, Hertz-damp, and Sears Models. These models are based on determining the force applied to the masses in numerical analysis by controlling the displacement or velocity difference [3, 10–14]. For this purpose, Anagnostopoulos [3] modelled adjacent buildings with single-degree-of-freedom and examined the pounding using spring-damper elements. In some earthquakes, it was revealed that while the damage was minor in the intermediate buildings, the percentage of destruction was higher in the corner buildings. Kumbasar [4] studied adjacent structures which have stories at the same level and considered these structures as shear frames for simplification. Only the spring element is used for the pounding model, and the damping is not taken into consideration. In the established model, the effects of collisions on structures with different periods according to the change in mass ratios were examined under the El Centro earthquake. In order to reduce the effects of a collision, it was suggested to use deformable elements in the earthquake joints. Zhang et al. [5] created a mechanical model with the matrix transfer method and compared the numerical data obtained with different analysis programs. They examined the pounding force, the number of pounding, the moment of pounding, and the structural displacements between two adjacent structures. They concluded that the pounding effects are sensitive to the change in peak ground acceleration and the size of the gap between buildings. Besides the pounding models used in numerical analysis, studies on the effects of seismic gaps between adjacent buildings, considering different parameters, were carried out by Saxena et al. [6]. In addition, Khatami et al. [7, 8], in their studies, investigated the effect of seismic gaps in the presence of lateral stiffness irregularity, soft stories, and regular and irregular adjacent structures using an experimental model of Takabatake et al. [9], which had two frames with single span and four-story. In another study, the adjacent buildings were modelled as multi-degree systems consisting of lumped masses, and the pounding was simulated using five different earthquake motions. Moreover, it was found that the collision caused high stresses when the structures had different heights, periods, or masses to a large extent [10]. In Jankowski's studies [11, 12], using spring and damper, the spring force was calculated using a non-linear viscoelastic pounding model to

simulate structural collision more precisely during earthquakes. The restitution coefficient formulation, which is a parameter related to the damping ratio, was obtained and verified. Miari and Jankowski [15] subjected two single-story steel building models to shaking table tests under scaled earthquakes for different seismic gaps and different soil types according to ASCE 7-10. In the study, they examined the effect of gap size and soil type on pounding by comparing the peak acceleration values in the models under different cases experimentally [15].

Athanassiadou et al. [16] parametrically examined the phase difference and pounding of adjacent single-degree-of-freedom systems with similar or different dynamic properties and revealed that rigid structures, like corner structures, are more affected. Naserkhaki et al. [17] used spring-damper elements for adjacent structures and showed that when the height of buildings differs significantly, the tall building is almost unaffected, while the short building is affected by the collision.

Luo et al. [18] compared the situations where dampers are connected and not connected between two adjacent buildings. As a result of the experiments with the shaking table, it is stated that the distance between the structures can be 30 cm under moderate and strong earthquakes and 24 cm under rare earthquakes in case the adjacent structures are not connected with the damper. In the case of the damper used, it was suggested that the seismic gap could be 10 cm under various performance conditions. Khan et al. [19] studied the seismic response of two adjacent fifteen- and ten-story buildings connected by a viscous damper. As a result of combining the structures of different frequencies with dampers, they showed that the earthquake-induced responses of the two buildings were reduced. In another study, passively controlled viscous dampers were used to reduce the response of explosion-induced vibrations in adjacent structures. It is stated that these dampers are efficient, and in different structures, the peak response is almost equivalent for bounded or unbounded structures [20].

Miari et al. [1], in their review article, studied previous research, including earthquake-induced structural pounding aiming to understand better the pounding phenomenon for the identification of parameters, soil interaction issues, mitigation measures, and recommended directions for future research studies on structural pounding. In one of their recommendations, they emphasized further studies to determine the effect of the impact stiffness and the coefficient of restitution on impact modelling for quantifying the parameters as indicated.

In this study, shake table experiments have been carried out with an innovative approach using the image processing technique to implement and determine pounding parameters. Numerical analyses of two adjacent three-story structure models were performed using the Kelvin–Voigt pounding model, one of the most common numerical pounding models. The numerical and experimental results are compared by performing shaking table tests under harmonic excitation and earthquake loads.

2. NUMERICAL METHOD FOR POUNDING ANALYSIS

In adjacent building models, the pounding effect is generally considered as the force generated in the pressure spring acting on the adjacent structure(s) as a reaction force by

controlling the displacement. Figure 1 shows a schematic representation of two 3-story shear frames and the distribution of Kelvin-Voigt models (Figure 2) between adjacent building models. The equations of motion at the moment of collision for these two shear frames are given separately in Equations (1) and (2).

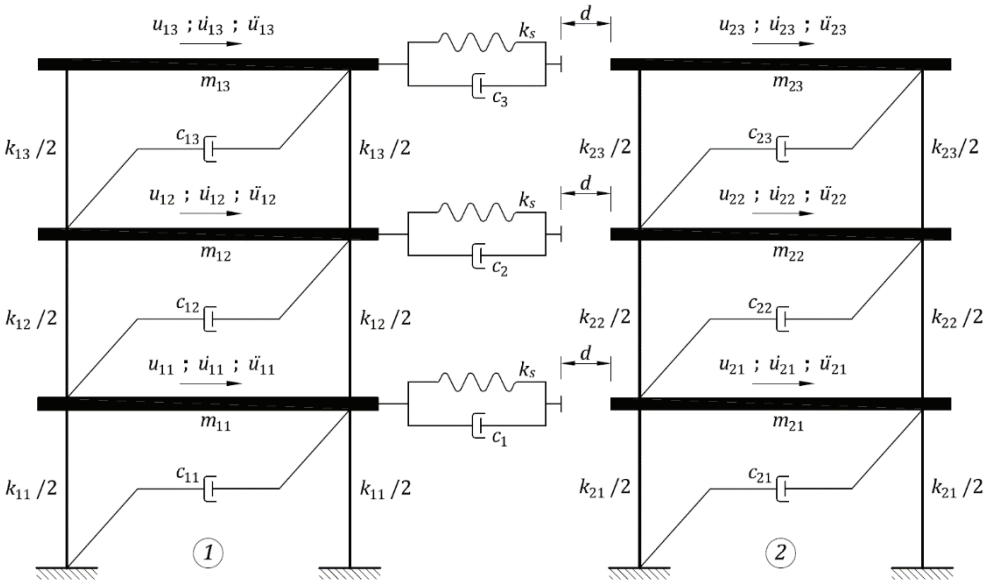

Figure 1 - Schematic representation of 3-story shear frames and distribution of Kelvin-Voigt Models

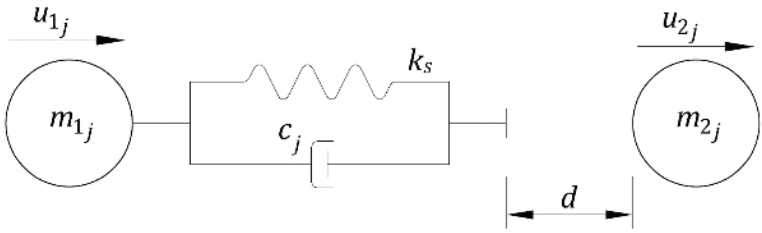

Figure 2 - Kelvin-Voigt Model [13]

$$\mathbf{M}_1\ddot{\mathbf{U}}_1+\mathbf{C}_1\dot{\mathbf{U}}_1+\mathbf{K}_1\mathbf{U}_1-\mathbf{F}=-\mathbf{M}_1\ddot{\mathbf{U}}_g \tag{1}$$

$$\mathbf{M}_2\ddot{\mathbf{U}}_2+\mathbf{C}_2\dot{\mathbf{U}}_2+\mathbf{K}_2\mathbf{U}_2+\mathbf{F}=-\mathbf{M}_2\ddot{\mathbf{U}}_g \tag{2}$$

$$\mathbf{M}_1=\begin{bmatrix} m_{11} & 0 & 0 \\ 0 & m_{12} & 0 \\ 0 & 0 & m_{13} \end{bmatrix}; \qquad \mathbf{K}_1=\begin{bmatrix} k_{11}+k_{12} & -k_{12} & 0 \\ -k_{12} & k_{12}+k_{13} & -k_{13} \\ 0 & -k_{13} & k_{13} \end{bmatrix};$$

$$\mathbf{C}_1=\begin{bmatrix} a_{10}m_{11}+a_{11}\left(k_{11}+k_{12}\right) & -a_{11}k_{12} & 0 \\ -a_{11}k_{12} & a_0 m_{12}+a_{11}\left(k_{12}+k_{13}\right) & -a_{11}k_{13} \\ 0 & -a_{11}k_{13} & a_{10}m_{13}+a_{11}k_{13} \end{bmatrix} \tag{3}$$

$$\mathbf{M}_2=\begin{bmatrix} m_{21} & 0 & 0 \\ 0 & m_{22} & 0 \\ 0 & 0 & m_{23} \end{bmatrix}; \qquad \mathbf{K}_2=\begin{bmatrix} k_{21}+k_{22} & -k_{22} & 0 \\ -k_{22} & k_{22}+k_{23} & -k_{23} \\ 0 & -k_{23} & k_{23} \end{bmatrix};$$

$$\mathbf{C}_2=\begin{bmatrix} a_{20}m_{21}+a_{21}\left(k_{21}+k_{22}\right) & -a_{21}k_{22} & 0 \\ -a_{21}k_{22} & a_{20}m_{22}+a_{21}\left(k_{22}+k_{23}\right) & -a_{21}k_{23} \\ 0 & -a_{21}k_{23} & a_{20}m_{23}+a_{21}k_{23} \end{bmatrix} \tag{4}$$

$$\ddot{\mathbf{U}}_1=\begin{bmatrix} \ddot{u}_{11} \\ \ddot{u}_{12} \\ \ddot{u}_{13} \end{bmatrix}; \qquad \dot{\mathbf{U}}_1=\begin{bmatrix} \dot{u}_{11} \\ \dot{u}_{12} \\ \dot{u}_{13} \end{bmatrix}; \qquad \mathbf{U}_1=\begin{bmatrix} u_{11} \\ u_{12} \\ u_{13} \end{bmatrix} \tag{5}$$

$$\ddot{\mathbf{U}}_2=\begin{bmatrix} \ddot{u}_{21} \\ \ddot{u}_{22} \\ \ddot{u}_{23} \end{bmatrix}; \qquad \dot{\mathbf{U}}_2=\begin{bmatrix} \dot{u}_{21} \\ \dot{u}_{22} \\ \dot{u}_{23} \end{bmatrix}; \qquad \mathbf{U}_2=\begin{bmatrix} u_{21} \\ u_{22} \\ u_{23} \end{bmatrix} \tag{6}$$

In Equations (1) and (2), $\mathbf{M_1}$ and $\mathbf{M_2}$ represent mass matrices, $\mathbf{K_1}$ and $\mathbf{K_2}$ stiffness matrices, and $\mathbf{C_1}$ and $\mathbf{C_2}$ damping matrices for shear frame models 1 and 2. Mass, damping, and stiffness matrices of the shear frames given by Model-1 and Model-2 are calculated by Equation (3) and Equation (4), respectively. With *i* representing the model number, the terms $\boldsymbol{a_{i0}}$ and $\boldsymbol{a_{i1}}$ in the damping matrices in Equations (3) and (4) are calculated according to Rayleigh Damping [21]. The vectors of acceleration ($\ddot{\mathbf{U}}_1$ and $\ddot{\mathbf{U}}_2$), velocity ($\dot{\mathbf{U}}_1$ and $\dot{\mathbf{U}}_2$), and displacement ($\mathbf{U_1}$ and $\mathbf{U_2}$) in Equations (1) and (2) are given in Equations (5) and (6). $\ddot{\mathbf{U}}_\mathbf{g}$ in Equations (1) and (2) represents the ground acceleration.

At the moment of collision, **–F** and **+F** forces act on the masses m_{1j} and m_{2j} at the floor levels, respectively, with *j* representing the floor number in both models. The force vector **F** given in Equation (7) includes the spring forces acting on the floor levels of the shear frames. The calculation of the pounding forces and the necessary boundary conditions are given in Equation (8). The pounding force to be used in the numerical analysis of the Kelvin-Voigt Model depends on two parameters, spring stiffness (k_s) and damping (c_j), as seen in Equation (8). Anagnostopoulos [3], for the simplified model of several adjacent structure analyses, uses the impact element stiffness as 0.01, 0.1, and 1.0 times the initial stiffness of an idealized

single-degree-of-freedom structure system. As seen in Equation (9), damping c_j varies depending on the spring stiffness k_s, damping ratio ξ_s, and m_{ij} story masses. The damping rate is related to a coefficient of restitution r, given in Equation (10). When $r = 1$, the damping ratio is $\xi_s = 0$, and the Model behaves linearly elastic, and when $r = 0$, the damping ratio takes the value $\xi_s = 1$. Khatiwada et al. [14] showed that the coefficient r could be taken as 0.4.

$$\mathbf{F} = \begin{bmatrix} F_{11} \\ F_{12} \\ F_{13} \end{bmatrix} = \begin{bmatrix} F_{21} \\ F_{22} \\ F_{23} \end{bmatrix} \tag{7}$$

$$\left.\begin{aligned} F_{1j} = F_{2j} &= 0 \\ F_{1j} = F_{2j} &= k_s\left(u_{1j} - u_{2j} - d\right) + c_j\left(\dot{u}_{1j} - \dot{u}_{2j}\right) \end{aligned}\right\} \begin{aligned} u_{1j} - u_{2j} - d &\le 0 \\ u_{1j} - u_{2j} - d &> 0 \end{aligned} \tag{8}$$

$$c_j = 2\xi_s\sqrt{k_s\frac{m_{1j}m_{2j}}{m_{1j}+m_{2j}}} \tag{9}$$

$$\xi_s = \frac{-\ln r}{\sqrt{\pi^2 + \left(\ln r\right)^2}} \tag{10}$$

In this study, numerical analyses were performed by the Newmark Mean Acceleration Method [21] using Matlab [22] program. Equations (11) and (12) are first calculated using the Newmark Mean Acceleration Method to obtain pounding forces under harmonic excitation and strong ground motion. Then, the spring damping ratio is calculated according to Equation (10) and its damping by Equation (9). At the beginning of the n^{th} time step, pounding forces are taken as F_{ij}= 0. The calculations are repeated through Equations (13) - (16) and analyzed in the time history. After calculating Equation (15), a contact check is performed to determine the pounding force at each time step. If any contact exists at any floor level, each floor's pounding force is calculated according to Equation (8), and then Equation (13) is repeated. At this stage, the displacement, velocity, and acceleration calculations are repeated for the $(n+1)^{\text{th}}$ step. The same operations are repeated throughout the time history by moving to the next time step (n+2).

$$\ddot{\mathbf{U}}_{i,0} = \mathbf{M}_i^{-1}\left(\mathbf{P}_{i,0} - \mathbf{K}_i\mathbf{U}_{i,0} - \mathbf{C}_i\dot{\mathbf{U}}_{i,0}\right) \tag{11}$$

$$\begin{aligned} &\mathbf{a}_{i,1} = \frac{1}{\beta\left(\Delta t\right)^2}\mathbf{M}_i + \frac{\gamma}{\beta\Delta t}\mathbf{C}_i; \quad \mathbf{a}_{i,2} = \frac{1}{\beta\Delta t}\mathbf{M}_i + \left(\frac{\gamma}{\beta}\text{-}1\right)\mathbf{C}_i; \\ &\mathbf{a}_{i,3} = \left(\frac{1}{2\beta}\text{-}1\right)\mathbf{M}_i + \left(\frac{\gamma}{2\beta}\text{-}1\right)\mathbf{C}_i; \end{aligned} \tag{12}$$

$$\hat{\mathbf{P}}_{i,n+1} = \mathbf{P}_{i,n+1} + \mathbf{a}_{i,1}\mathbf{U}_{i,n+1} + \mathbf{a}_{i,2}\dot{\mathbf{U}}_{i,n} + \mathbf{a}_{i,3}\ddot{\mathbf{U}}_{i,n} \mp \mathbf{F}_{n+1} \tag{13}$$

$$\mathbf{U}_{i,n+1} = \hat{\mathbf{K}}_i^{-1}\hat{\mathbf{P}}_{i,n+1} \tag{14}$$

$$\dot{\mathbf{U}}_{i,n+1} = \frac{\gamma}{\beta\Delta t}\left(\mathbf{U}_{i,n+1} - \mathbf{U}_{i,n}\right) + \left(1 - \frac{\gamma}{\beta}\right)\dot{\mathbf{U}}_{i,n} + \Delta t\left(1 - \frac{\gamma}{2\beta}\right)\ddot{\mathbf{U}}_{i,n} \tag{15}$$

$$\ddot{\mathbf{U}}_{i,n+1} = \frac{\gamma}{\beta\left(\Delta t\right)^2}\left(\mathbf{U}_{i,n+1} - \mathbf{U}_{i,n}\right) - \left(1 - \frac{\gamma}{\beta\Delta t}\right)\dot{\mathbf{U}}_{i,n} - \left(\frac{\gamma}{2\beta} - 1\right)\ddot{\mathbf{U}}_{i,n} \tag{16}$$

3. EXPERIMENTAL STUDY

Two 3-story building models shown in Figure 1 were built to compare with the results obtained from the numerical analysis. The total height of the two identical building models designed is 1000 mm. 8 mm thick Medium-Density-Fiberboard (MDF) material was used for the floor slabs, and M6 rods were used for the columns. Slab areas are 200x200 mm^2. The ends of the columns were connected with fiber nuts at the bottom and top points of the slabs, and it was tried to ensure the fixed-end connection between the slab and the column to achieve the ideal shear frame behavior. In order to create a pounding on two identical building models, their periods were changed by adding additional mass to the stories of Model-1.

Within the scope of the study, only the cases where the floor alignments are at the same level were examined (Figure 3). Representing the situation where the seismic gaps are insufficient, the two structural models are positioned adjacently on the shaking table SARSAR [23]. Experimental studies are first carried out under harmonic excitation and then earthquake simulations. For harmonic experiments, free vibration and forced vibration tests with a shaking table were carried out to determine the dynamic characteristics of each structural Model, such as period, mode shape, and damping ratio.

In earthquake simulations, it is necessary to scale the ground motion according to the capacities of the shaking tables in a way that preserves the peak accelerations and spectrum characteristics. Therefore, considering the displacement-time record of the Düzce earthquake used in the experiments and the displacement limit (±75 mm) of the shaking table SARSAR, the motion data was scaled at 1/15. Scaling was performed with equations 17-19 using the method proposed by Harris and Sabnis [24]. Here λ_L, λ_T, λ_A represent displacement, time, and acceleration scales, respectively. In this scaling, by dividing the earthquake time history by $15^{1/2}$, the characteristics of the peak accelerations and response spectrum can be preserved. In another way, this scaling means that considering the positions of the measured periods of the experimental models Model-1 (T_1= 0.233 s) and Model-2 (T_1= 0.138 s) on the scaled spectrum, they represent actual structures with first periods of 0.233x15$^{0.5}$= 0.90 and 0.138x15$^{0.5}$= 0.53 seconds.

$$\lambda_A = \frac{\lambda_L}{\lambda_T^2} = 1 \tag{17}$$

$$\lambda_L = \lambda_T^2 \tag{18}$$

$$\lambda_T = \sqrt{\lambda_L} \tag{19}$$

White Light-Emitting-Diode (LED) markers are placed on the stories of each Model and shaking table to obtain motion information with the image processing technique. Each video frame was processed separately to track the white LEDs. In order to distinguish the white LEDs from the other objects in the video frames, the B component of the RGB video frames, considered as the first step, was converted to greyscale and filtered according to the brightness threshold value of I= 0.99. Pixels above the threshold value were converted to white, and those below the threshold value were converted to black. Different filtering functions in MATLAB [22] were used to convert the unrelated white pixels to black, if any exist in the video frame, except for the LEDs to be tracked. In addition, to determine the coordinates of the center of the LEDs, a median filter was applied to soften the geometry of the white LED pixel areas. By repeating the same operations for each frame, the displacement-time history of the LEDs is obtained.

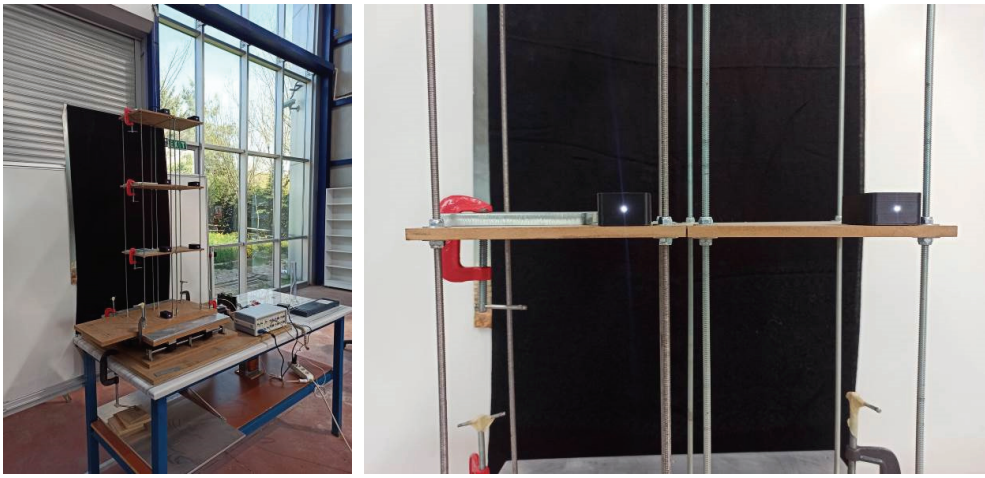

Figure 3 - General view of the experimental setup (left) and LED markers placed on the floors (right)

The displacements in pixels of the white LEDs, tracked through video recordings, were recorded in the time domain. The obtained pixel-time histories were used to determine the mode shapes and dominant frequencies of the building models with Fast Fourier Transform (FFT). In numerical analyses, the initial lateral stiffness for each story ($4(12EI_c/L^3)$) is calculated using M6 rods' minor thread diameter (4.77 mm) as 6.83 kN/m where the initial flexural stiffness of columns was taken as EI_c= 5.4 Nm^2. By the obtained experimental results, taking into consideration the first mode resonance frequency (f_1) of each structure model, the model update procedure was applied to each numerical Model. Modifying the flexural stiffness of columns ensured that the numerical models and the experimental results were compatible. According to the experimental results, the final lateral stiffness of Model-

1 and Model-2 are calculated as 5.92 kN/m and 5.14 kN/m, respectively. Masses, initial, and final flexural stiffnesses compatible with the test models are given in Table 1. Before each experiment, due to changes in ambient conditions such as temperature and humidity, possible changes in the modal frequencies of the models are checked from video recordings by FFT.

Table 1- Masses and stiffnesses of the test models

Story	Model-1 f_1= 4.28 Hz, ξ= %1.05			Model-2 f_1= 7.22 Hz, ξ= %1.07		
	Mass [kg]	Initial EI_c [Nm^2]	Final EI_c [Nm^2]	Mass [kg]	Initial EI_c [Nm^2]	Final EI_c [Nm^2]
1	1.7	5.4	4.6	0.56	5.4	4.1
2	1.7	5.4	4.6	0.56	5.4	4.1
3	1.6	5.4	4.6	0.45	5.4	4.1

Videos were recorded at 100, 500, and 1000 fps using a Sony RX100M5 camera, and the pounding durations were determined at recording rates of 10, 2, and 1 millisecond, respectively, by image processing to observe dynamic behavior and pounding. Data obtained by these recording rates were compared among each other, and it was concluded that they were compatible. The experimental studies were carried out with a recording rate of 100 fps.

In addition, the accelerations were measured and recorded with ARDUINO-based low-cost accelerometers at the top floor level during simulations under earthquake to observe pounding. These accelerometers are manufactured using a mems type MPU6050 sensor and ARDUINO NANO.

4. COMPARISON OF EXPERIMENTAL AND NUMERICAL RESULTS

The image processing results obtained by the shaking table experiments were compared with the numerical results of the shear frames, where pounding forces were determined by the Kelvin-Voigt model under the effect of harmonic excitation and strong ground motion. In Figure 4, the displacement responses obtained from the 3rd floor of both models by image processing of the video recordings taken under harmonic excitation with ±2 mm amplitude and 6 Hz frequency are given. For comparison purposes, cases for the different spring stiffness and damping ratios of the Kelvin-Voigt model are considered in the numerical analyses, and the optimum spring stiffness and damping ratio for both building models are investigated. In numerical simulations, based on the initial shear stiffness (k= 6.83 kN/m) of a single story, the cases where the ratio of spring stiffness k_s to shear stiffness k is considered as 10, 5, 1, 0.1 times in the dashpot model and these cases are used for the comparison with the coefficient of restitution r which is taken as 1.0, 0.8, 0.6, 0.4 and 0.2. Figures 5-8 show comparisons of the numerical analyses to the experimental results using different spring stiffnesses and coefficient of restitution r. Sub-space-plots (SSP) were created to examine the relationship between experimental and numerical results for different spring stiffnesses. In each case, the relationships due to the variation of coefficient of restitution r are given in

Figures 9-12. The errors caused by the amplitude and phase differences can be easily examined in these graphs. In Figure 13, where the spring stiffness of the Kelvin-Voigt Model is taken equal to the initial story shear stiffness, $k_s = k$=6.83 kN/m and compared to experimental results is interpreted as the most acceptable case for both models. For Model-1 and Model-2, when the r coefficient is taken as 0.2 or 0.4, numerical results were determined to be close to the experimental results. Regarding these findings, variation of k_s according to coefficients of restitution r for 0.2 and 0.4 are given in Figures 13 and 15. When the SSP graphs given in Figures 14 and 16 are examined, it is seen that acceptable results are obtained in cases where the spring stiffness is k, 5k, or 10k according to these coefficients of restitution.

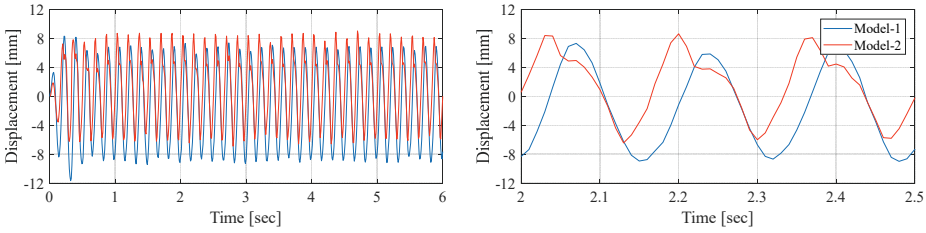

Figure 4 - Relative displacements obtained from the 3rd floor of both models by image processing (±2 mm @ 6 Hz). Displacement-time series of both models (left), and the displacements for 2-2.5 seconds time interval (right).

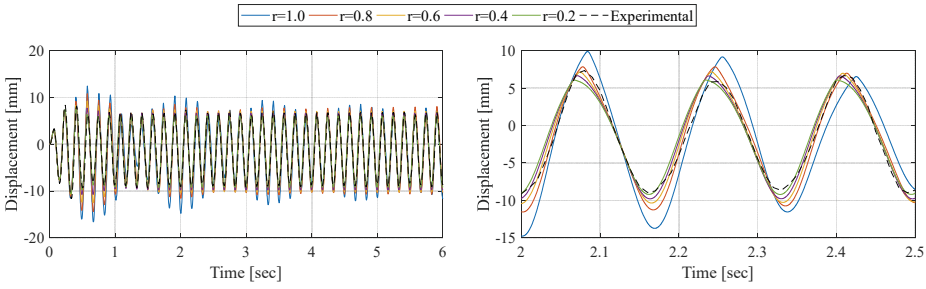

a) Model-1

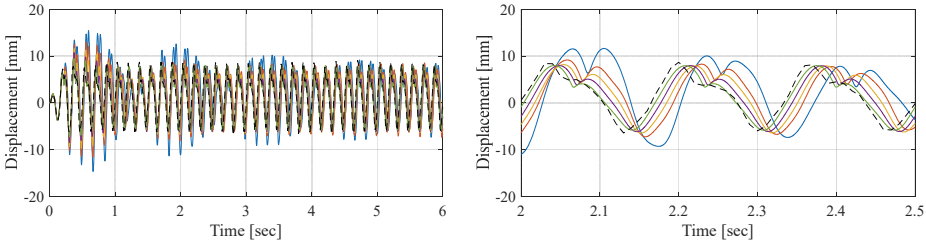

b) Model-2

Figure 5 - Relative displacement-time histories of Model-1 (a) and Model-2 (b) for the case k_s=10k (±2 mm @ 6 Hz). Displacement-time series of both models (left), and the displacements for 2-2.5 seconds time interval (right).

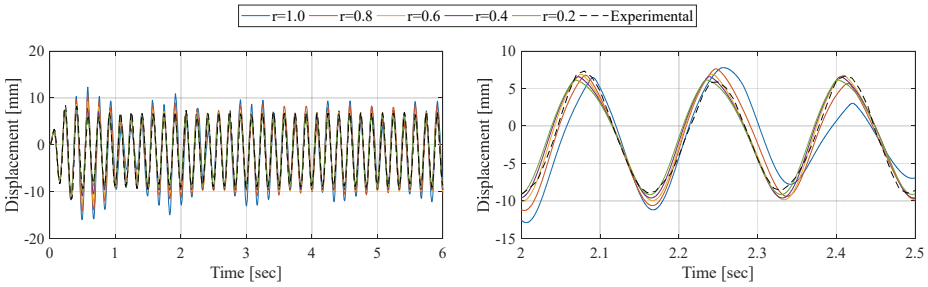

a) Model-1

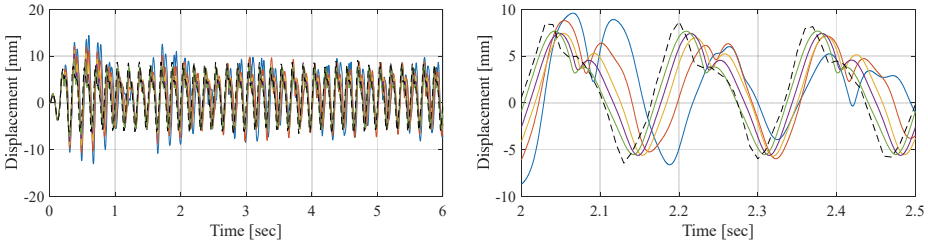

b) Model-2

Figure 6 - Relative displacement-time histories of Model-1 (a) and Model-2 (b) for the case k_s=5k (±2 mm @ 6 Hz). Displacement-time series of both models (left), and the displacements for 2-2.5 seconds time interval (right).

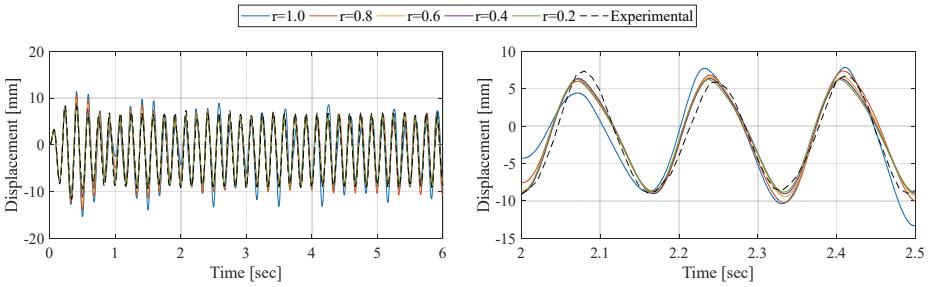

a) Model-1

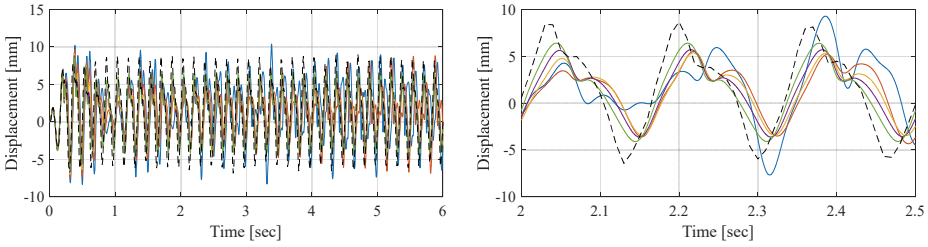

b) Model-2

Figure 7 - Relative displacement-time histories of Model-1 (a) and Model-2 (b) for the case k_s=k (±2 mm @ 6 Hz). Displacement-time series of both models (left), and the displacements for 2-2.5 seconds time interval (right).

The reasons why the results do not match exactly, even in the most favorable situation, could be explained as; (i) that an ideal shear frame could not be obtained in the experimental structural models, (ii) surface defects in colliding structure stories causing local contact rather than surface contact in pounding, (iii) the contact surface changes during a collision due to possible torsional effects in 3D structural models.

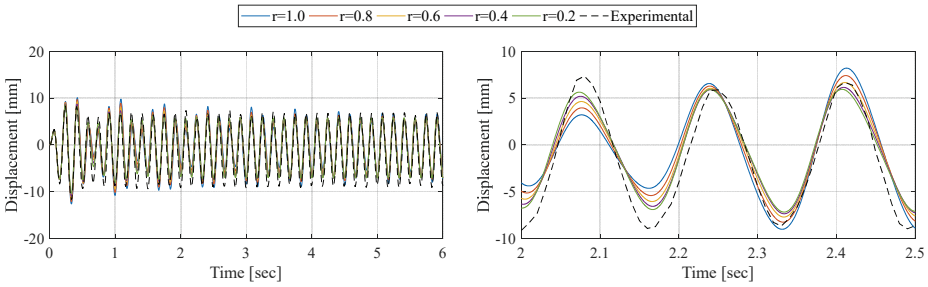

a) Model-1

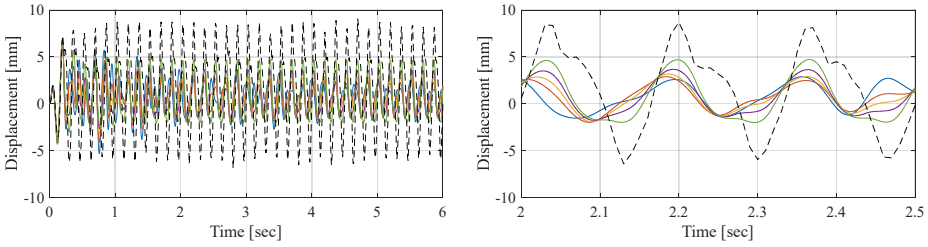

b) Model-2

Figure 8 - Relative displacement-time histories of Model-1 (a) and Model-2 (b) for the case k_s=0.1k (±2 mm @ 6 Hz). Displacement-time series of both models (left), and the displacements for 2-2.5 seconds time interval (right).

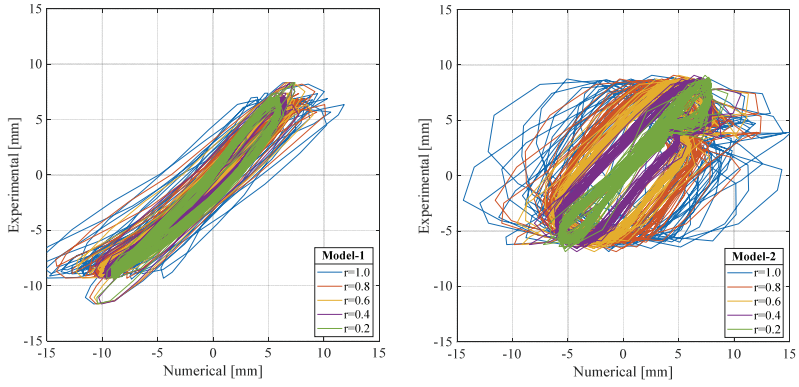

Figure 9 - SSP of experimental and numerical simulations for k_s=10k (±2 mm @ 6 Hz) with different coefficients of restitution r.

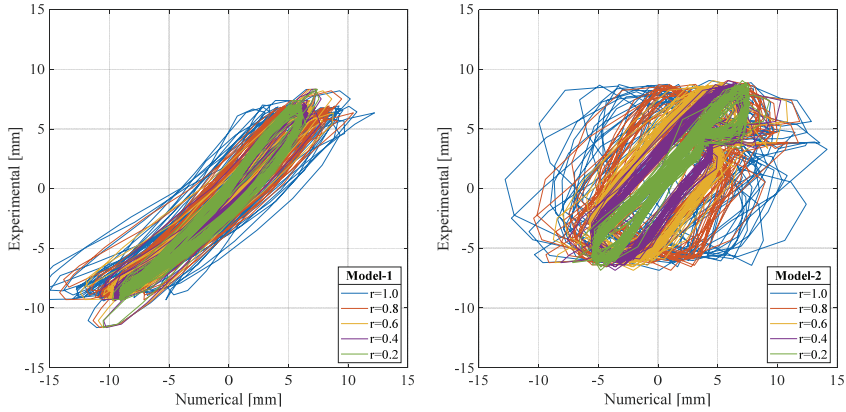

Figure 10 - SSP of experimental and numerical simulations for k_s=5k (±2 mm @ 6 Hz) with different coefficients of restitution r.

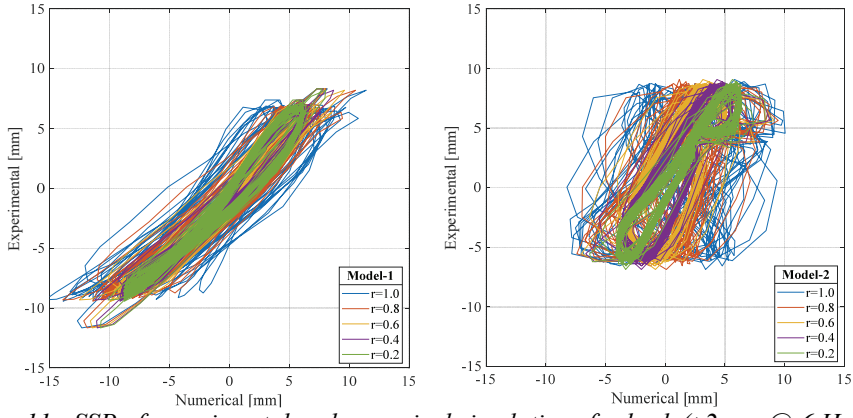

Figure 11 - SSP of experimental and numerical simulations for k_s=k (±2 mm @ 6 Hz) with different coefficients of restitution r.

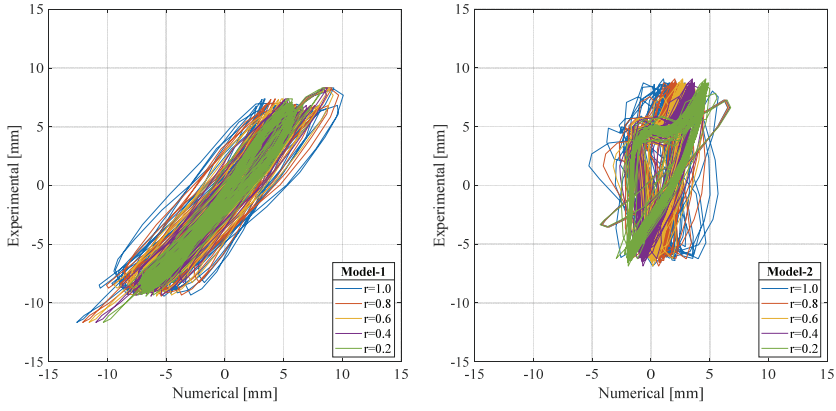

Figure 12 - SSP of experimental and numerical simulations for k_s=0.1k (±2 mm @ 6 Hz) with different coefficients of restitution r.

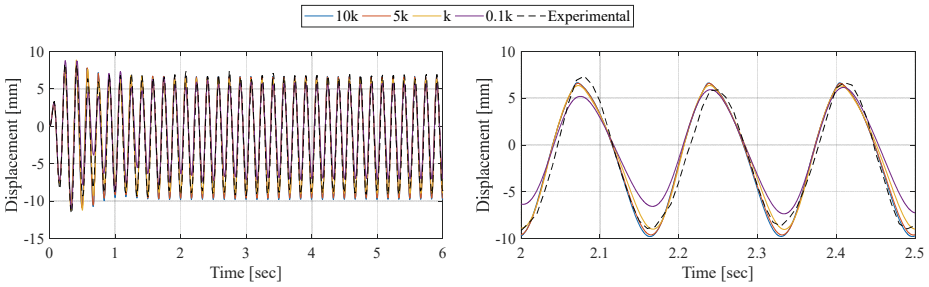

a) Model-1

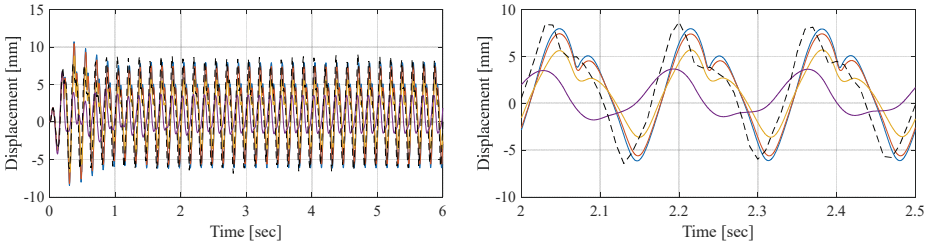

b) Model-2

Figure 13 - Comparison of the effect of spring stiffness on relative displacement-time histories of Model-1 (a) and Model-2 (b), for r= 0.4 (±2 mm @ 6 Hz). Displacement-time series of both models (left), and the displacements for 2-2.5 seconds time interval (right).

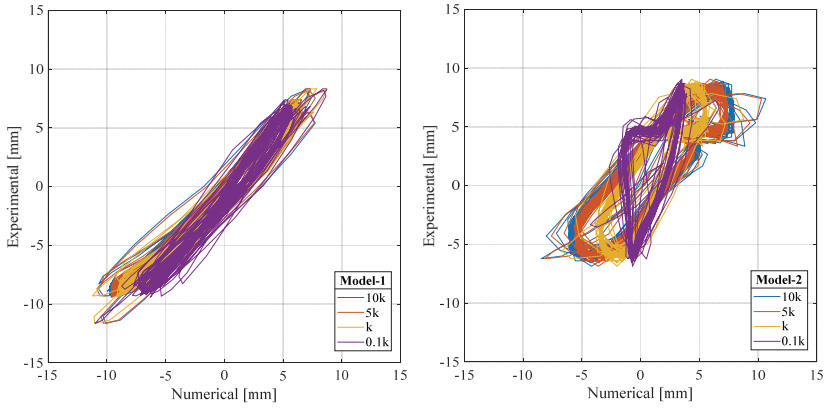

Figure 14 - SSP of experimental and numerical simulations for r= 0.4 (±2 mm @ 6 Hz) with different k_s.

In addition, the displacement results obtained by image processing under ±1 mm harmonic motion at 4.613 Hz, which is the achieved frequency by the shake table for near the resonance frequency of Model-1, are given in Figure 17 for Model-1 and Model-2. Numerical analysis and experimental results examining the spring stiffness by accepting the coefficient of

restitution as r= 0.4 are given in Figure 18. When the numerical analysis results under harmonic excitation are examined, it is seen that the ideal results are obtained where the ratio of spring stiffness to shear stiffness (k_s/k) is 1, 5, or 10.

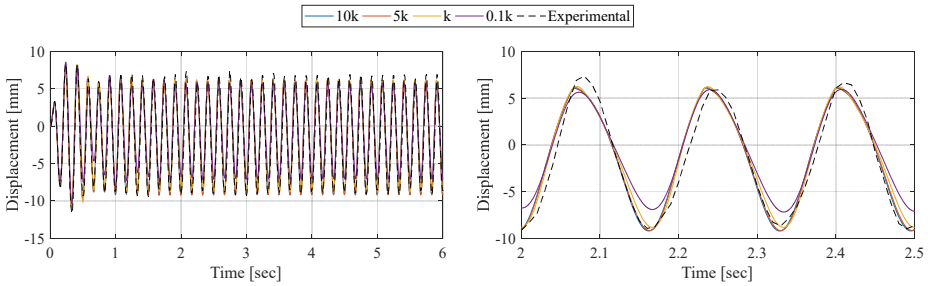

a) Model-1

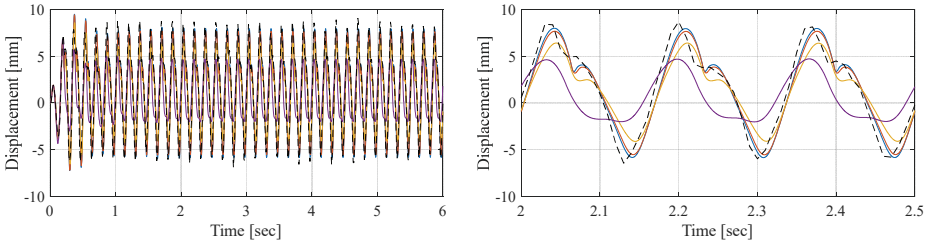

b) Model-2

Figure 15 - Comparison of the effect of spring stiffness on relative displacement-time histories of Model-1 (a) and Model-2 (b), for r= 0.2 (±2 mm @ 6 Hz). Displacement-time series of both models (left), and the displacements for 2-2.5 seconds time interval (right).

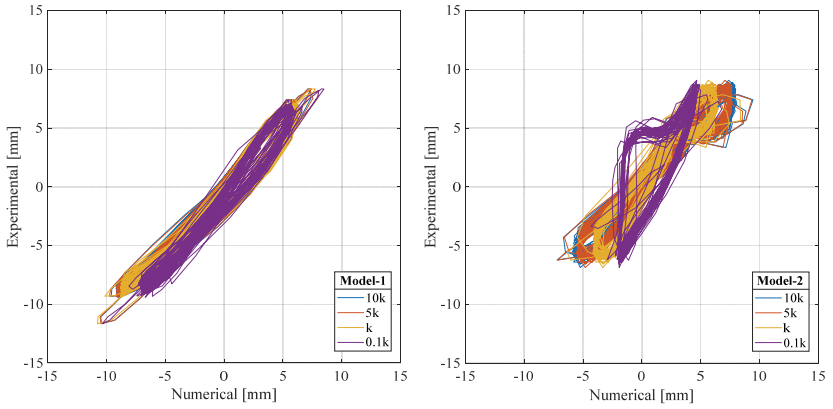

Figure 16 - SSP of experimental and numerical simulations for r= 0.2 (±2 mm @ 6 Hz) with different k_s.

In the numerical analysis, the force F_{13}= F_{23}, which occurs during pounding between 3rd floor masses, is given in Figure 19, and it is calculated around 28 N at the maximum when r= 0.4 and the spring stiffness is equal to the shear stiffness (k_s= k= 6.83 kN/m). It was calculated in numerical studies that the contact time during pounding varies between approximately 20-25 milliseconds, while in experimental studies, this period was observed between 50-60 milliseconds (Figure 4).

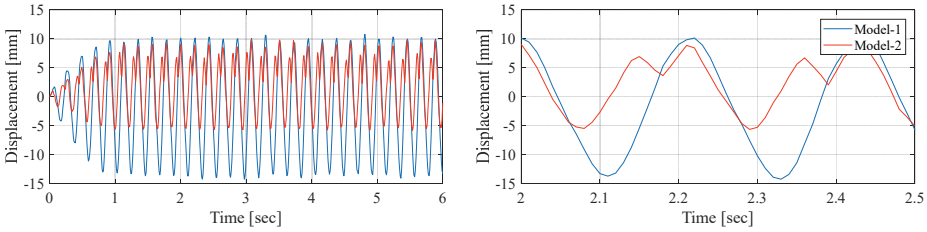

Figure 17 - Relative displacements obtained from the 3rd floor of both models by image processing (±1 mm @ 4.613 Hz) Displacement-time series of both models (left), and the displacements for 2-2.5 seconds time interval (right).

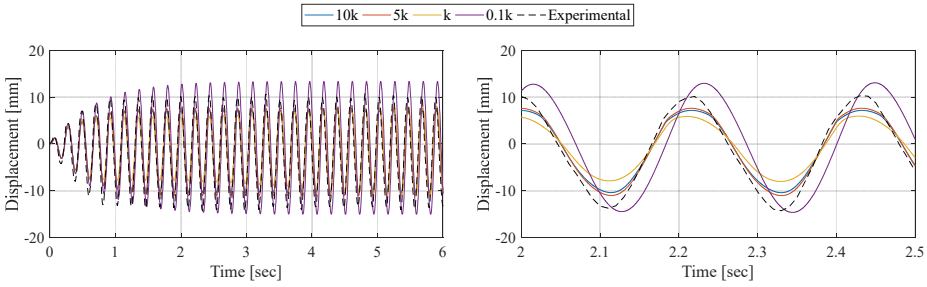

a) Model-1

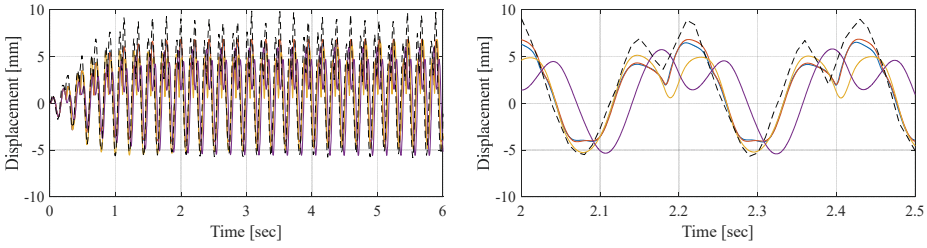

b) Model-2

Figure 18 - Comparison of the effect of spring stiffness on relative displacement-time histories of Model-1 (a) and Model-2 (b), for r= 0.4 (±1 mm @ 4.613 Hz). Displacement-time series of both models (left), and the displacements for 2-2.5 seconds time interval (right).

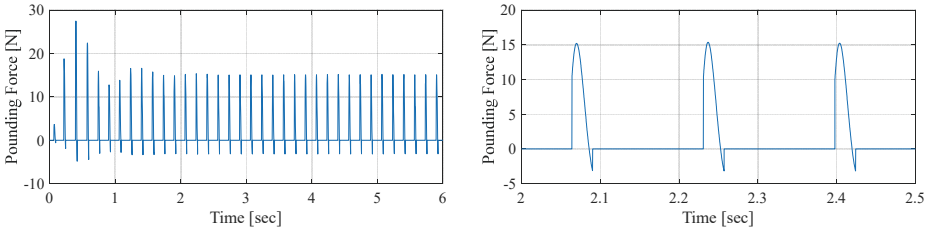

Figure 19 - Pounding forces $F_{13} = F_{23}$ for r= 0.4 and k_s=k (±2 mm @ 6 Hz) in time series (left), and the displacements for 2-2.5 seconds time interval (right).

In order to examine the pounding under the earthquake, shaking table tests were carried out using the 1999 Düzce earthquake record. Displacements were scaled to 1/15, and to keep peak accelerations the same, time was scaled to $15^{1/2}$, considering the ±75 mm displacement capacity of the shaking table [23]. In the earthquake simulation, acceleration and video recording were taken, and the cases where the models are adjacent and separate were examined comparatively. In Figure 20, the filtered acceleration responses of the 3rd floor are given for both models. It was seen that while the pounding increases the acceleration responses for Model-1, the acceleration responses decrease for Model-2 in the time history. The peak acceleration obtained for Model-1 increased from 1.23g to 1.41g by 14.63%. For Model-2, the peak acceleration remained the same at 1.48g.

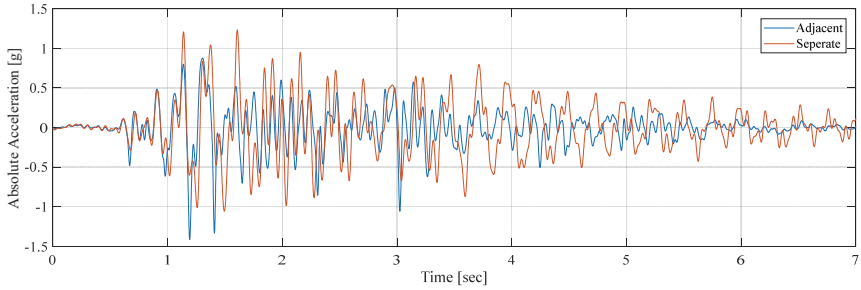

a) Model-1

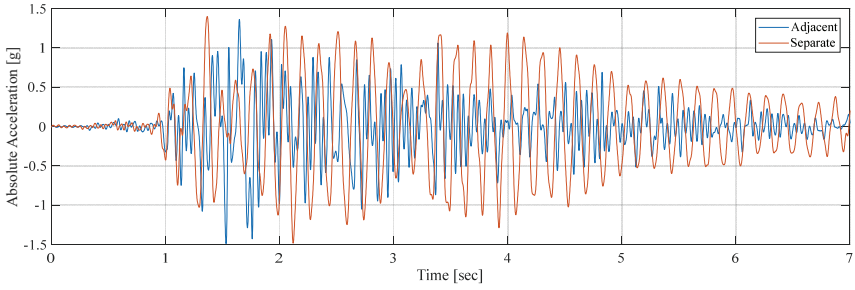

b) Model-2

Figure 20 - Comparison of acceleration responses on Model-1 (a) and Model (2) for adjacent and separated cases

Appropriate coefficient of restitution (r) and stiffness ratio (k_s/k) is investigated by relative root-mean-square (RMS) error [25] of numerical and experimental displacement time-histories using Equation (20).

$$\varepsilon_{rel} = \frac{\sqrt{(1/N)\Sigma_{n=1}^{N}(x_d[n]-x_e[n])^2}}{\sqrt{(1/N)\Sigma_{n=1}^{N}(x_e[n])^2}} \times 100 \tag{20}$$

The relative RMS errors, ε_{rel} calculated with Equation (20) between the numerical (x_d) and the experimental (x_e) displacements are listed in Tables 2 and 3 for Model-1 and Model-2, respectively. Minimum relative RMS errors of 42.41% and 52.62%, which are the most congruent results, are obtained for $k_s/k = 5$ at $r = 0.2$ and $r = 0.4$. Even though these values represent the best result, considering the SSPs obtained from harmonic tests, earthquake simulations with the combination of 1, 5, and 10 stiffness ratios with 0.2, 0.4, and 0.6 coefficients of restitution are also interpreted as acceptable. For this reason, an investigation is carried out on the peak displacements obtained from experimental results with numerical peak displacements considering these r and k_s/k combinations. The differences in peak displacement for Model-1 and Model-2 are listed in Table 4, where the peak experimental displacement for Model-1 is 13.21 mm at 1.40 sec and for Model-2 is 6.93 mm at 1.29 sec. Considering these comparisons, the most congruent results are obtained for $k_s/k = 1$ and $r = 0.2$. The r and k_s/k combinations, except those given in Table 4, were not taken into consideration because of the incompatible time intervals corresponding to peak displacements in the numerical analysis compared to the actual behavior observed by experiments.

Table 2 - Relative RMS error percentages of experimental and numerical analysis results depending on r and k_s/k ratios for Model-1

k_s/k \ r	**0.2**	**0.4**	**0.6**	**0.8**	**1.0**
0.1	56.34	68.24	89.11	127.65	198.94
1	42.94	45.00	64.66	86.28	161.08
5	43.74	**42.41**	45.83	73.67	127.07
10	43.76	43.53	55.41	82.97	139.79

Table 3 - Relative RMS error percentages of experimental and numerical analysis results depending on r and k_s/k ratios for Model-2

k_s/k \ r	**0.2**	**0.4**	**0.6**	**0.8**	**1.0**
0.1	80.08	92.07	114.25	150.70	252.73
1	54.63	57.79	82.34	124.31	241.61
5	**52.62**	54.57	65.62	107.32	198.68
10	53.65	57.21	67.94	104.42	181.04

Table 4 - Comparison of numerical peak displacements with experimental peak displacements for Model-1 and Model-2

	Model-1 (13.21 mm, t = 1.40 sec)						**Model-2** (6.93 mm, t = 1.29 sec)					
	***r*= 0.2**		***r*= 0.4**		***r*= 0.6**		***r*= 0.2**		***r*= 0.4**		***r*= 0.6**	
k_s/k	Disp. [mm]	Diff. [%]	Disp. [mm]	Diff. [%]	Disp. [mm]	Diff. [%]	Disp. [mm]	Diff. [%]	Disp. [mm]	Diff. [%]	Disp. [mm]	Diff. [%]
1	13.31	**-0.79**	13.52	-2.37	13.59	-2.87	7.48	**-7.93**	7.89	-13.85	8.41	-21.36
5	13.37	-1.23	13.51	-2.31	14.18	-7.34	7.71	-11.35	8.22	-18.74	8.97	-29.44
10	13.39	-1.39	13.66	-3.41	14.14	-7.04	7.68	-10.90	8.19	-18.30	9.14	-31.89

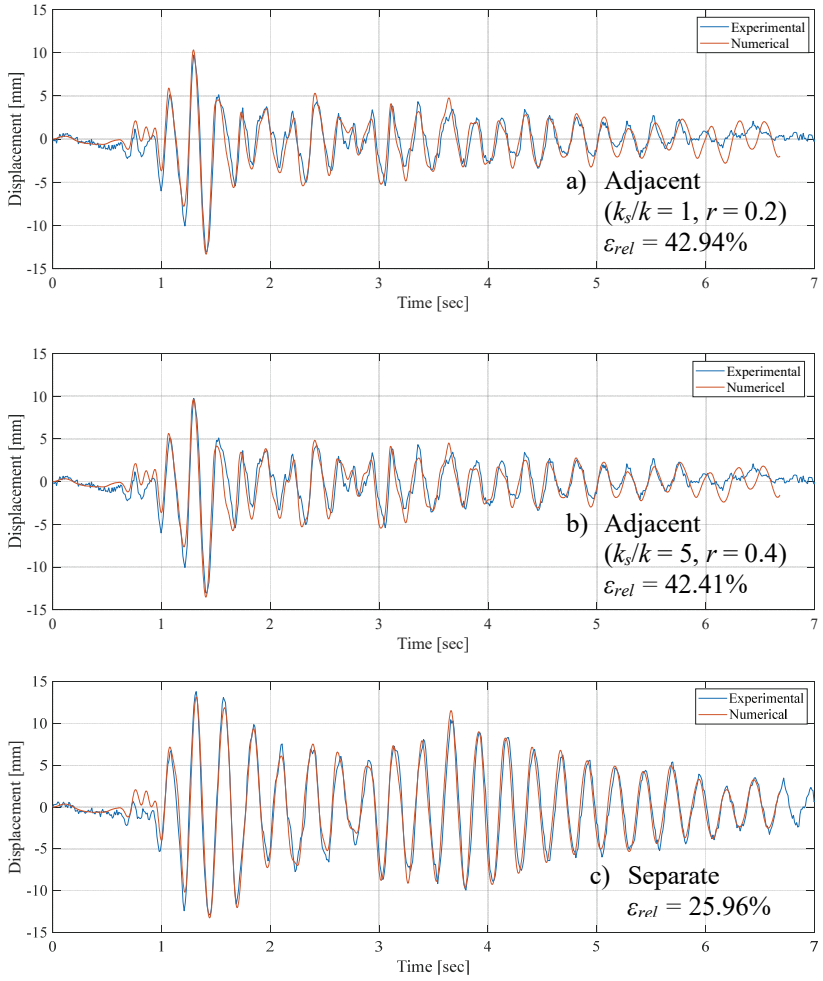

Figure 21 - Comparison of relative displacement-time histories of Model-1 for experimental and numerical results. Adjacent cases (a) and (b), separated case (c).

Time history analysis to observe pounding using the most congruent results plotted with experimental results are given in Figure 21 for Model-1 and Figure 22 for Model-2. Figures 21(a) and 22(a) show the adjacent state for $k_s/k = 1$ and $r = 0.2$ for Model-1 and Model-2, respectively. Figures 21(b) and 22(b) show the adjacent state for $k_s/k = 5$ and $r = 0.4$ for Model-1 and Model-2, respectively. For the case of the sufficient seismic gap, where the building models placed separately, experimental and numerical displacement time-history responses are shown in Figures 21(c) and 22(c). While peak displacements are 13.8 mm for Model-1 and 8.95 mm for Model-2, an apparent change in the time domain for the case of the insufficient seismic gap is observed under earthquake simulation. Peak displacements were decreased by 4.27% for Model-1 and 22.57% for Model-2.

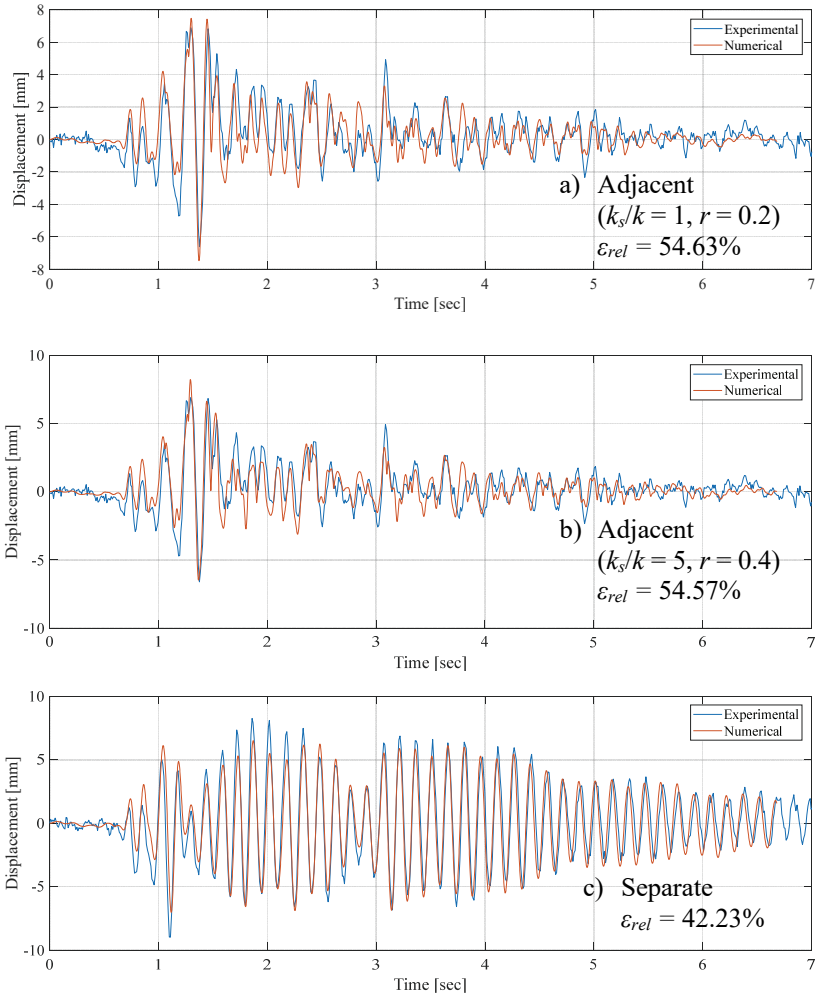

Figure 22 - Comparison of relative displacement-time histories of Model-2 for experimental and numerical results. Adjacent cases (a) and (b), separated case (c).

5. CONCLUSIONS

Performing collision effects with real-scale experiments is very difficult and require significant investments. Therefore, to determine the compatibility of numerical pounding models and parameters with the actual structure behavior, it is necessary to conduct experimental studies on scaled structure models in the laboratory environment.

In this study, numerical analyses using the Kelvin-Voigt pounding model and their comparison with the displacement responses obtained from the experiments carried out by the image processing technique are presented to examine the pounding in adjacent structures. Harmonic excitation tests are evaluated with relative RMS errors of earthquake simulations to investigate the performance of the Kelvin-Voigt pounding model. The results obtained in the study are as follows:

- With the experimental studies, it has been concluded that the pounding phenomena can be observed, and collision durations can be measured by video recordings with a frequency of 100 fps.
- When compared with the experimental results, it is seen that the Kelvin-Voigt pounding model gives relevant results under both harmonic and earthquake effects. Still, experimental studies are needed to determine the spring and damping parameters. It is beneficial to diversify such experimental studies due to the variety of parameters and manufacturing and material defects in the experimental models.
- Considering the complexity of the problem, it is clear that a perfect result in full compliance with the experiments cannot be obtained. Differences between the model analyzed under ideal conditions, and the experimental model also have an effect on the pounding simulations. This situation can also be observed in the time-history graphics obtained from earthquake tests on the models in separate cases. Even without the pounding effect, the relative RMS errors were obtained as 25.96% and 42.23% for Model-1 and Model-2.
- Tests for the cases when the coefficient of restitution is taken as $r = 0.2$ or 0.4, and the ratio of spring stiffness to shear stiffness (k_s/k) is 1, 5, or 10 in harmonic excitations give the most congruent results with numerical simulations. In earthquake simulations, using the differences in peak displacement and relative RMS errors, it has been experienced that cases for $r = 0.2$ with $k_s/k = 1$, and $r = 0.2$ or $r = 0.4$ with $k_s/k = 5$ are interpreted as the most reasonable results. However, considering relative RMS errors of 42.41% and 52.62% (>30%) shows that the relation between experimental and numerical results has a poor concordance. Therefore, further experimental and numerical research is being recommended better to determine the effectiveness of the numerical pounding models.
- When adjacent and separate states are examined under the effect of the earthquake, it is observed that the peak displacements are decreased by 4.27% for Model-1 and 22.57% for Model-2 in the adjacent state compared to the separate state. Besides the peaks, a significant decrease in displacements is also observed in the time domain.

- In earthquake simulation, pounding phenomena caused an increase in peak acceleration by 14.63% for Model-1, while the peak acceleration on Model-2 remained the same for the adjacent state.
- The results obtained by experiments specific to building models investigated in this study, performed harmonic excitation and earthquake tests, show that the image processing technique is a successful method for examining the pounding phenomena. In particular, this technique can be used practically to update the finite element models of structures and to determine or verify the parameters such as spring stiffness and damping and the collision durations of mathematical pounding models.

Symbols

c_{1j}, c_{2j} : Damping of the j^{th} story of Model-1 and Model-2

c_j : Damping of the j^{th} story in Kelvin-Voigt Model

$\mathbf{C_1}$, $\mathbf{C_2}$: Damping matrix of Model-1 and Model-2

E : Elasticity modulus

EI_c : Flexural stiffness

f_1 : First mode frequency of models

F_{ij} : Pounding force for the j^{th} story of Model-i

$\mathbf{F}$: Pounding force vector of Kelvin-Voigt Model

I_c : Moment of inertia for column

I : Brightness threshold value

i : Model number index

j : Model story index

k : Story shear stiffness

k_s : Spring stiffness

k_{1j}, k_{2j} : j^{th} story shear stiffness of Model-1 and Model-2

$\mathbf{K_1}$, $\mathbf{K_2}$: Stiffness matrix of Model-1 and Model-2

L : Height of story for models

$\mathbf{M_1}$, $\mathbf{M_2}$: Mass matrix of Model-1 and Model-2

m_{1j}, m_{2j} : j^{th} story lumped masses of Model-1 and Model-2

n : Step number for Newmark Mean Acceleration Method and time-history

N : Total number of samples

r : Coefficient of restitution

T_1 : First mode period of models

u_{1j}, u_{2j} : j^{th} story displacement of Model-1 and Model-2

$\mathbf{U_1}$, $\dot{\mathbf{U}}_1$, $\ddot{\mathbf{U}}_1$: Vectors of displacement, velocity, and acceleration for Model-1

$\mathbf{U_2}$, $\dot{\mathbf{U}}_2$, $\ddot{\mathbf{U}}_2$: Vectors of displacement, velocity, and acceleration for Model-2

$\ddot{\mathbf{U}}_\mathbf{g}$: Ground acceleration

x_e : Experimental displacement

x_d : Numerical displacement

Δt : Timestep

β : Parameter in Newmark's method

γ : Parameter in Newmark's method

ε_{rel} : Relative root mean square error

ξ : Damping ratio of Model-1 and Model-2

ξ_s : Damping ratio of Kelvin-Voigt model

λ_A : Acceleration scale

λ_L : Displacement scale

λ_T : Time scale

References

[1] Miari, M., Choong, K. K., Jankowski, R., Seismic pounding between adjacent buildings: Identification of parameters, soil interaction issues and mitigation measures, *Soil Dynamics and Earthquake Engineering*, 121, 135-150, 2019. doi: 10.1016/j.soildyn.2019.02.024.

[2] Turkish Building Earthquake Code (TBEC). Turkish Ministry of Environment and Urbanisation, Ankara, 2018.

[3] Anagnostopoulos, S. A., Pounding of buildings in series during earthquakes, *Earthquake Engineering & Structural Dynamics*, 16(3), 443–456, 1988. doi: 10.1002/eqe.4290160311.

[4] Kumbasar, N., Collision Problem of Shear Frames During Earthquakes (in Turkish), *Teknik Dergi*, 4(16), 609–617, 1993.

[5] Zhang, Y., Ding, J., Zhuang, H., Chang, Y., Chen, P., Zhang, X., Xie, W., Fan, J., Pounding between Adjacent Frame Structures under Earthquake Excitation Based on Transfer Matrix Method of Multibody Systems, *Advances in Civil Engineering*. 2019. doi: 10.1155/2019/5706015.

[6] Saxena, N., Ghosh, R., Debbarma, R., Analysis of seismic separation gap between two adjacent reinforced concrete buildings, *AIP Conference Proceedings*, 2019: 2158(September). doi: 10.1063/1.5127126.

[7] Khatami, M., Gerami, M., Kheyroddin, A., Siahpolo, N., The Effect of Irregularity of Lateral Stiffness in Estimating the Separation Gap of Adjacent Frames, *KSCE Journal of Civil Engineering*, 24(1), 166–177, 2020. doi: 10.1007/s12205-020-0173-4.

[8] Khatami, M., Gerami, M., Kheyroddin, A., Siahpolo, N., The Effect of the Mainshock-Aftershock on the Estimation of the Separation Gap of Regular and Irregular Adjacent Structures with the Soft Story, *Journal of Earthquake and Tsunami*, 14(2), 1–25, 2020. doi: 10.1142/S1793431120500086.

[9] Takabatake, H., Yasui, M., Nakagawa, Y. and Kishida, A., Relaxation method for pounding action between adjacent buildings at expansion joint, *Earthquake Engineering & Structural Dynamics*, 43(9), 1381–1400, 2014. doi: 10.1002/eqe.2402.

[10] Anagnostopoulos, S.A., Spiliopoulos, K.V., An investigation of earthquake induced pounding between adjacent buildings, *Earthquake Engineering & Structural Dynamics*, 21(4), 89–302, 1992. 2doi: 10.1002/eqe.4290210402.

[11] Jankowski, R., Non-linear viscoelastic modelling of earthquake-induced structural pounding, *Earthquake Engineering and Structural Dynamics*, 34(6), 595–611, 2005. doi: 10.1002/eqe.434.

[12] Jankowski, R., Analytical expression between the impact damping ratio and the coefficient of restitution in the non-linear viscoelastic model of structural pounding, *Earthquake Engineering and Structural Dynamics*, 35(4), 517–524, 2006. doi: 10.1002/eqe.537.

[13] Kharazian, A., López-Almansa, F., State-of-the-Art of Research on Seismic Pounding Between Buildings with Aligned Slabs, *Archives of Computational Methods in Engineering*, 26(2), 327–345, 2019. doi: 10.1007/s11831-017-9242-3.

[14] Khatiwada, S., Chouw, N., Butterworth, J.W., Evaluation of numerical pounding models with experimental validation, *Bulletin of the New Zealand Society for Earthquake Engineering*, 46(3), 117–130, 2013. doi: 10.5459/bnzsee.46.3.117-130.

[15] Miari, M., Jankowski, R., Shaking table experimental study on pounding between adjacent structures founded on different soil types, *Structures*, 44, 851-879, 2022. doi:10.1016/j.istruc.2022.08.059.

[16] Athanassiadou, C.J., Penelis, G.G., Kappos, A.J., Seismic Response of Adjacent Buildings with Similar or Different Dynamic Characteristics, *Earthquake Spectra*, 10(2), 293–317, 1994. doi: 10.1193/1.1585775.

[17] Naserkhaki, S., Abdul Aziz, F.N.A., Pourmohammad, H., Parametric study on earthquake induced pounding between adjacent buildings, *Structural Engineering and Mechanics*, 43(4), 503–526, 2012. doi: 10.12989/sem.2012.43.4.503.

[18] Luo, H., Wu, Q., Pan, W., Research and Experiment on Optimal Separation Distance of Adjacent Buildings Based on Performance, *Mathematical Problems in Engineering,* 2018. doi: 10.1155/2018/3483401.

[19] Khan, S., Kumar, C.L.M., Shwetha, K.G., Analytical study on the seismic behavior of two adjacent buildings connected by viscous dampers, *AIP Conference Proceedings*, 2020. doi: 10.1063/1.5141540.

[20] Kangda, M.Z., Bakre, S., Response control of adjacent structures subjected to blast-induced vibrations, *In Proceedings of the Institution of Civil Engineers: Structures and Buildings*, 172(12), 2019. doi: 10.1680/jstbu.18.00071.

[21] Chopra, A.K., *Dynamics of structures: Theory and applications to earthquake engineering*, Prentice Hall, 1995.

[22] Matlab. Versiyon 2017b. Natick: The MathWorks, Inc.

[23] Damcı, E., Şekerci, Ç., Development of a Low-Cost Single-Axis Shake Table Based on Arduino, *Experimental Techniques*, 43(2), 179–198, 2019. doi: 10.1007/s40799-018-0287-5.

[24] Harris H.G., Sabnis G.M., *Structural modeling and experimental techniques*, 2nd edn., CRC Press, 1999.

[25] Luco, J.E., Ozcelik, O., Conte, J.P., Acceleration Tracking Performance of the UCSD-NEES Shake Table, *Journal of Structural Engineering*, 136(5), 481-490, 2010. doi: 10.1061/(ASCE)ST.1943-541X.0000137